

Inverse Edelstein effect induced by magnon-phonon couplingMingran Xu,¹ Jorge Puebla,^{2,*} Florent Auvray,¹ Bivas Rana,² Kouta Kondou,² and Yoshichika Otani^{1,2,†}¹*Institute for Solid State Physics, University of Tokyo, 5-1-5 Kashiwanoha, Kashiwa, Chiba 277-8581, Japan*²*CEMS, RIKEN, Saitama 351-0198, Japan*

(Received 16 February 2018; revised manuscript received 7 April 2018; published 10 May 2018)

We demonstrate a spin to charge current conversion via magnon-phonon coupling and an inverse Edelstein effect on the hybrid device Ni/Cu(Ag)/Bi₂O₃. The generation of spin current ($J_s \approx 10^8$ A/m²) due to magnon-phonon coupling reveals the viability of acoustic spin pumping as a mechanism for the development of spintronic devices. A full in-plane magnetic field angle dependence of the power absorption and a combination of longitudinal and transverse voltage detection reveals the symmetric and asymmetric components of the inverse Edelstein effect voltage induced by Rayleigh-type surface acoustic waves. While the symmetric components are well studied, asymmetric components still need to be explored. We assign the asymmetric contributions to the interference between longitudinal and shear waves and an anisotropic charge distribution in our hybrid device.

DOI: [10.1103/PhysRevB.97.180301](https://doi.org/10.1103/PhysRevB.97.180301)

Methods for the generation of spin current and its conversion to electrical charge current has been vigorously studied in recent years, particularly based on physical phenomena at the nanoscale [1]. In the presence of magnetic materials, spin currents can be generated by magnon-photon or magnon-phonon coupling. Magnon-phonon coupling can be achieved by passing surface acoustic waves (SAWs) across ferromagnetic layers due to the magnetoelastic effect [2]. A periodic elastic deformation of ferromagnetic films by SAW drives precessional magnetization dynamics such as ferromagnetic resonance (FMR). This process is known as acoustic-FMR (A-FMR), and is analogous to the most common FMR, which is driven by electromagnetic waves (photons). Both FMR and A-FMR are used as mechanisms for the generation of spin current which can be injected into adjacent nonmagnetic layers, a process better known as spin pumping [3,4]. The generated spin current is usually converted to electrical charge current by the inverse spin Hall effect (ISHE) [5]. Alternatively, recent reports showed efficient spin to charge current conversion at interfaces with spatial inversion asymmetry between two nonmagnetic materials [6,7]. Spatial inversion asymmetry induces a built-in electric potential and spin-orbit coupling at the surfaces and interfaces, the so-called Rashba spin-orbit coupling [8]. Here, the spin to charge conversion mechanism is known as the inverse Edelstein effect (IEE). In this Rapid Communication, we demonstrate spin to charge conversion in a hybrid device which combines magnon-phonon coupling via SAW and IEE.

Our hybrid devices consist of a Ni(10 nm)/Cu(20 nm)/Bi₂O₃(20 nm) and Ni(10 nm)/Ag(20 nm)/Bi₂O₃(20 nm) trilayer structures deposited on LiNbO₃ substrates at the center of a pair of Ti(5 nm)/Au(20 nm) interdigital transducers (IDTs). By applying rf voltage at the input IDT, Rayleigh-type SAWs are launched along the x axis [see Fig. 1(a)], driving a time-dependent strain field $\varepsilon(t)$ in the lattice, inducing a

time-varying contribution to the magnetic anisotropy in the ferromagnetic layer (Ni) via the magnetoelastic effect [2]. As schematically demonstrate in Fig. 1(b), in the presence of a static magnetic field \mathbf{H} , the SAW-induced anisotropy field excites a precessional motion of magnetization \mathbf{M} around the \mathbf{H} direction, enabling ferromagnetic resonance in Ni and injecting spin current into the adjacent nonmagnetic layer, Cu (Ag). Then, due to the inversion spatial symmetry breaking at the interface between Cu (Ag) and Bi₂O₃ [6,9,10], the system converts spin current into charge current via IEE, inducing a magnetic-field-dependent voltage V , detected in longitudinal and transverse geometries.

The spin current generated by SAW via magnon-phonon coupling strongly depends on the absorption of acoustic waves in the ferromagnetic layer. We first characterize the absorption of SAW by using a vector network analyzer (VNA) while varying the in-plane external magnetic field angle. The absorption of SAW is characterized by systematically measuring the transmission coefficient $|S_{21}|$ as a function of the in-plane static magnetic field magnitude and angle θ , as illustrated in Fig. 1(a). Figures 2(a) and 2(b) show the magnetic field angle dependence (θ) at the resonance peak of the absorption of SAW into FMR excitation in Ni. We observe a fourfold butterfly-shaped signal with the first maximum located at $\theta = 45^\circ$. Previous reports showed a fourfold symmetric dependence of SAW absorption with the angle formed between the SAW \mathbf{k} -wave vector and the in-plane magnetic field, having a maximum absorption at 45° , and which is considered to be a fingerprint of acoustic-FMR [2,11]. The asymmetry between the top and bottom sides of the fourfold symmetry indicates the non-negligible interference of magnetoelastic couplings of shear waves and longitudinal waves [Fig. 2(b)]. The magnetization dynamics induced by Rayleigh SAW is composed of longitudinal wave and shear wave motion components perpendicular to each other ($\pi/2$ dephasing), forming ellipsoidal oscillations. When the SAW direction vector \mathbf{k} is reversed, the ellipsoidal motion is reversed, which is accompanied by a sign change of the shear strain component ε_{zx0} . Magnetoelastic coupling

*jorgeluis.pueblanunez@riken.jp

†yotani@issp.u-tokyo.ac.jp

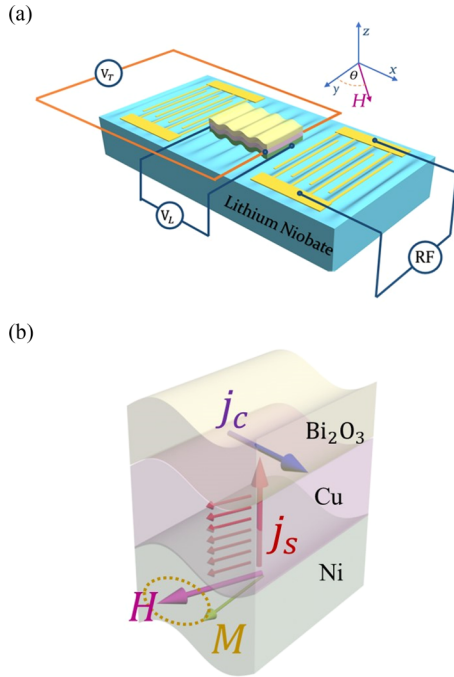


FIG. 1. (a) Illustration of the experiment setup. The surface acoustic waves are generated by applying rf voltage on interdigital transducers, and the longitudinal and transverse voltages are measured while applying an external magnetic field \mathbf{H} at an angle θ . (b) Schematics of the acoustic spin pumping mechanism and spin to charge conversion via IEE.

by interference of a longitudinal (ε_{xx0}) and shear wave (ε_{zx0}) can be described by Eq. (1), which directly elucidates the excitation efficiency of FMR, which is proportional to the SAW absorption $\Delta P(\theta) \propto [\mu_0 h_{\text{rf}}(\theta)]^2$,

$$[\mu_0 h_{\text{rf}}(\theta)]^2 = [b_1 \varepsilon_{xx0} \sin \theta \cos \theta + 2b_2 \varepsilon_{zx0} \sin \theta]^2, \quad (1)$$

where $b_{1(2)}$ is the magnetoelastic coupling constant, $\varepsilon_{xx0(zx0)}$ represents the longitudinal strain (shear strain) induced by SAW, and θ refers to the in-plane static magnetic field orientation as depicted in Fig. 1(a). Recently, the microscopic origin of this asymmetric mechanism has been reported and it has been ascribed to the simultaneous breaking of time reversal and spatial inversion symmetries [12]. Both time reversal and spatial inversion symmetry are broken on our hybrid device. The resultant asymmetry is particularly evident for Ni/Ag/Bi₂O₃ in Fig. 2(b). The ratio of longitudinal and transverse magnetoelastic coupling in Ag is larger than Cu, inducing larger anisotropies [13].

The driving of acoustic-FMR produces a spin current which can be injected into adjacent nonmagnetic layers, and converted to a charge current when a spin-orbit interaction occurs. Figure 3 shows the magnetic-field-dependent IEE charge current detected in Ni/Cu/Bi₂O₃ (red circles) and Ni/Ag/Bi₂O₃ (blue triangles) devices, rescaled by their corresponding SAW power absorption P_{SAW} . The spin to charge conversion at nonmagnetic metal/Bi₂O₃ interfaces was first reported by Karube *et al.* [6], describing the nonequilibrium spin accumulation induced by spin current injection at this interface, resulting in a shift of Fermi contours in momentum

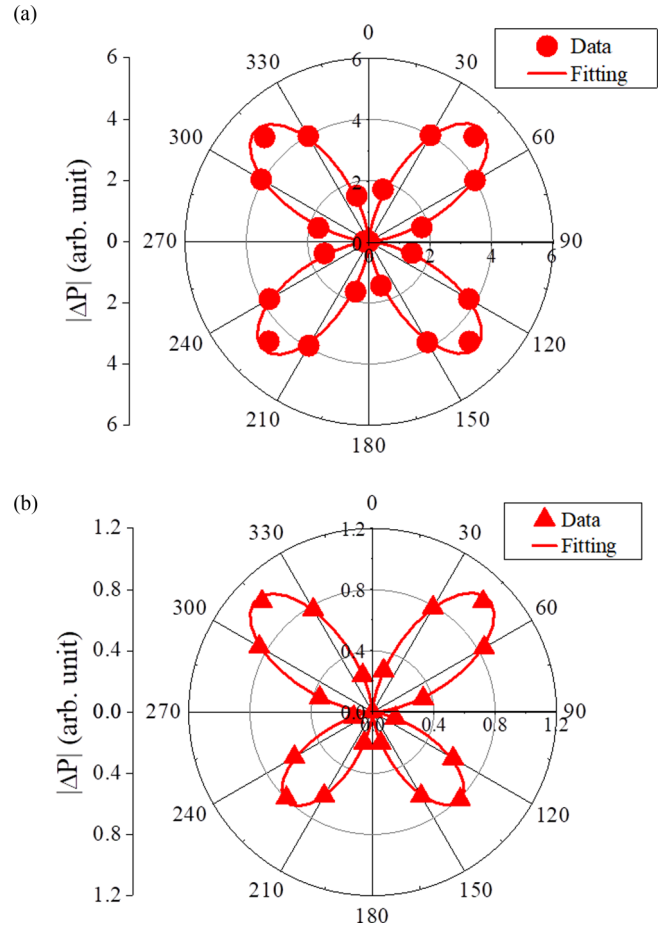


FIG. 2. Polar graph of damping of SAW due to acoustically excited FMR measured on (a) Ni/Cu/Bi₂O₃ and (b) Ni/Ag/Bi₂O₃, varying applied magnetic field angle θ .

space that generates a flow of charge current in the device. Considering the fact that the ISHE is negligible in our device, the spin pumping signal is mainly a consequence of the IEE. Therefore, the opposite sign of the spin pumping signal shown

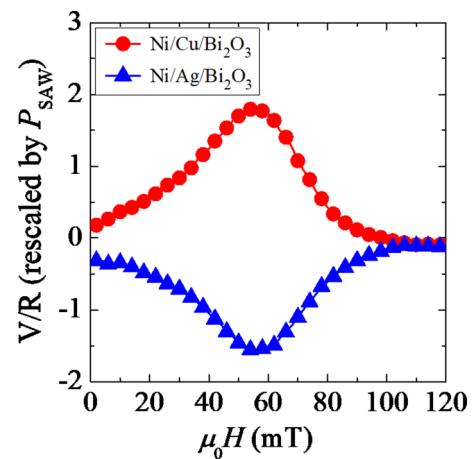


FIG. 3. Longitudinal signal measured on Ni/Cu/Bi₂O₃ (red circles) and Ni/Ag/Bi₂O₃ (blue triangles) devices depending on the magnetic field amplitude at $\theta = 240^\circ$.

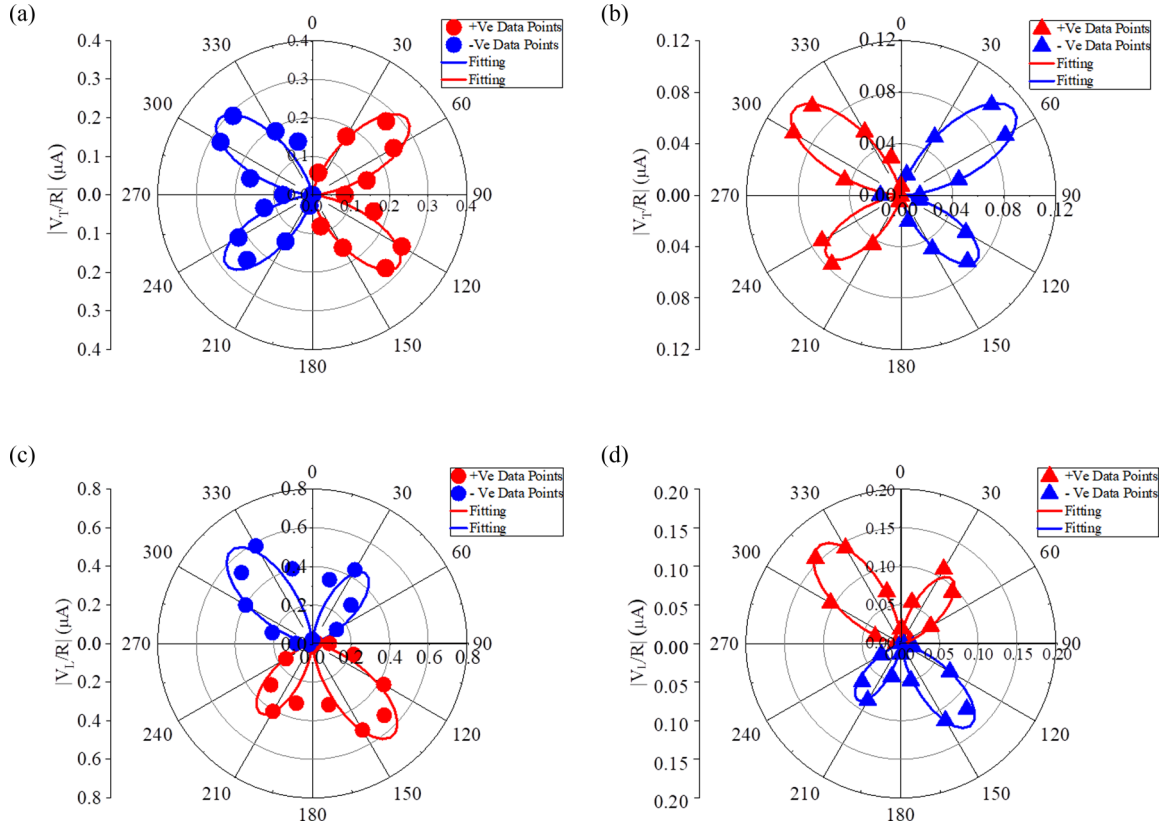


FIG. 4. Polar graph of the transverse signal measured on (a) Ni/Cu/Bi₂O₃ and (b) Ni/Ag/Bi₂O₃, varying the applied external magnetic field angle θ . Polar graph of the longitudinal signal measured on (c) Ni/Cu/Bi₂O₃ and (d) Ni/Ag/Bi₂O₃, varying the applied external magnetic field angle θ .

in Fig. 3 reflects the opposite spin momentum locking configuration at the Cu/Bi₂O₃ and Ag/Bi₂O₃ interfaces, corroborating well the observations from electromagnetic-wave-induced spin pumping and the magneto-optical Kerr effect (MOKE) [9,14]. Spin pumping measurements driven by electromagnetic wave FMR contain an asymmetric component due to the classical induction effect, the anisotropic magnetoresistance voltage [15]. The induction effect is strongly suppressed in acoustic spin pumping measurements.

The feasibility of acoustic spin pumping was previously reported in a limited range of in-plane magnetic field angles, measured in transverse geometry [4]. We extend our study to the full in-plane magnetic field angle dependence with voltage detection in both transverse and longitudinal geometries. For transverse geometry we detect the voltage perpendicular to the SAW wave vector \mathbf{k} [V_T in Fig. 1(a)], while for the longitudinal geometry we detect the voltage parallel to the SAW wave vector \mathbf{k} [V_L in Fig. 1(a)]. Figures 4(a) and 4(b) show the magnetic field angle dependence (θ) of the transverse IEE voltage V_T for Ni/Cu/Bi₂O₃ [Fig. 4(a)] and Ni/Ag/Bi₂O₃ [Fig. 4(b)]. Since the V_T mainly depends on the excitation efficiency of FMR and the projection angle of the spin current onto the Rashba interface, the top and bottom side asymmetry presented in SAW absorption is also reflected in the transverse voltage. For fitting our data, as the SAW damping in longitudinal direction does not affect the transverse potential in our device, the longitudinal component of $\mu_0 h_{rf}(\theta)$ has a negligible influence in our spin pumping signal, and we can only consider the transverse

component of excitation $|\mu_0 h_{rf}| \sin(\theta)$ in (2),

$$V_T(\theta)/R = C_1 [\mu_0 h_{rf}]^2 \sin(\theta). \quad (2)$$

We repeat our acoustic spin pumping measurements now with longitudinal voltage detection. Figures 4(c) and 4(d) show the magnetic field angle dependence (θ) of the longitudinal IEE voltage V_L for Ni/Cu/Bi₂O₃ [Fig. 4(c)] and Ni/Ag/Bi₂O₃ [Fig. 4(d)]. Due to the damping of SAW in the propagation direction, it is possible to observe the influence of the transverse excitation component in the V_L , adding an amplitude asymmetry in the fourfold symmetry. We fit our data by the following equation,

$$V_L(\theta)/R = [\mu_0 h_{rf}]^2 [C_T \sin(\theta) + C_L \cos(\theta)]. \quad (3)$$

We also observe an additional asymmetric component in Figs. 4(c) and 4(d). This asymmetric component is described by the nonsymmetric charge distribution at the position of our electrodes, when varying the magnetic field angle. The charge distribution is dictated by the electric field \mathbf{E} induced by a spin-orbit interaction, which is proportional to the flow direction of spin current J_s and its spin polarization σ_s , such that $\mathbf{E} \propto J_s \times \sigma_s$ [16]. Hence, the asymmetry is the result of the projection of spin polarization σ_s in transverse and longitudinal geometries and the damping of SAW in the propagation direction (see Supplemental Material [17]).

The magnitude of spin current generated via magnon-phonon coupling in our samples can be estimated by [7]

$$J_s = \frac{V(\theta)}{\lambda_{\text{IEE}} w R \sin \theta}, \quad (4)$$

where λ_{IEE} is the IEE length, w is the sample width, and R the electric sample resistance. For our Cu/Bi₂O₃ we have $\lambda_{\text{IEE}} = -0.17$ nm [14], $w = 10$ μm , $R = 42.87$ Ω . We obtain a spin current $J_s = 1.648 \times 10^8$ A/m² for $V_T(60^\circ)$ of Cu/Bi₂O₃ in Fig. 4(a). This spin current density is comparable to commonly reported values for standard spin pumping driven by electromagnetic wave FMR [7,18,19]. The full angle dependence of spin current is available in the Supplemental Material [17].

In summary, we have demonstrated the feasibility of combining acoustic spin pumping via magnon-phonon coupling and spin to charge conversion via IEE at the Rashba-like Cu(Ag)/Bi₂O₃ interfaces. The opposite signs of acoustic spin pumping signals elucidate the opposite spin configuration for Cu/Bi₂O₃ and Ag/Bi₂O₃ interfaces. A combination of full angle dependence of an in-plane magnetic field with transverse and longitudinal voltage detection allows one to study the contributions of longitudinal and shear waves always present in Rayleigh-type SAWs. Such contributions are observed as asymmetries present in the magnetic field dependence of absorption and acoustic spin pumping measurements. The

present study gives a systematic study of the mechanical generation of spin current via magnon-phonon interactions. Alternatively, it has been proposed that the mechanical generation of spin current can also be achieved by direct coupling to the atomic lattice, with no need for magnetic materials, external magnetic fields, and spin-orbit interactions [20]. An experimental manifestation of this coupling has been recently observed by coupling SAW to a Cu layer [21]. Despite the fact that our experimental scheme cannot rule out an additional generation of spin current via direct SAW coupling to our nonmagnetic layers (Cu, Ag), we do not observe clear evidence of it in our power absorption measurements at $\theta = 90^\circ$ or 270° , where the magnetization in Ni is expected to be perpendicular to the vector of spin polarization induced by spin rotation coupling (Fig. 2). This is the configuration for the maximum signal reported in Ref. [21]. The unambiguous determination of spin current generation by direct spin rotation coupling in Cu (Ag) may be achieved by optical characterization of spin accumulation without the presence of magnetic materials [9].

This work was supported by a Grant-in-Aid for Scientific Research on Innovative Area, “Nano Spin Conversion Science” (Grant No. 26103002) and RIKEN Incentive Research Project Grant No. FY2016. F.A. was supported by the Ministry of Education, Culture, Sports, Science and Technology (MEXT) Scholarship, Japan.

-
- [1] Y. Otani, M. Shiraishi, A. Oiwa, E. Saitoh, and S. Murakami, *Nat. Phys.* **13**, 829 (2017).
- [2] M. Weiler, L. Dreher, C. Heeg, H. Huebl, R. Gross, M. S. Brandt, and S. T. B. Goennenwein, *Phys. Rev. Lett.* **106**, 117601 (2011).
- [3] Y. Tserkovnyak, A. Brataas, and G. E. W. Bauer, *Phys. Rev. B* **66**, 224403 (2002).
- [4] M. Weiler, H. Huebl, F. S. Goerg, F. D. Czeschka, R. Gross, and S. T. B. Goennenwein, *Phys. Rev. Lett.* **108**, 176601 (2012).
- [5] O. Mosendz, V. Vlamincik, J. E. Pearson, F. Y. Fradin, G. E. W. Bauer, S. D. Bader, and A. Hoffmann, *Phys. Rev. B* **82**, 214403 (2010).
- [6] S. Karube, K. Kondou, and Y. Otani, *Appl. Phys. Express* **9**, 033001 (2016).
- [7] J. C. Rojas-Sánchez, L. Vila, G. Desfonds, S. Gambarelli, J. P. Attané, J. M. De Teresa, C. Magén, and A. Fert, *Nat. Commun.* **4**, 2944 (2013).
- [8] Y. Ando and M. Shiraishi, *J. Phys. Soc. Jpn.* **86**, 011001 (2017).
- [9] J. Puebla, F. Auvray, M. Xu, B. Rana, A. Albouy, H. Tsai, K. Kondou, G. Tatara, and Y. Otani, *Appl. Phys. Lett.* **111**, 092402 (2017).
- [10] J. Kim, Y.-T. Chen, S. Karube, S. Takahashi, K. Kondou, G. Tatara, and Y. C. Otani, *Phys. Rev. B* **96**, 140409(R) (2017).
- [11] L. Dreher, M. Weiler, M. Pernpeintner, H. Huebl, R. Gross, M. S. Brandt, and S. T. B. Goennenwein, *Phys. Rev. B* **86**, 134415 (2012).
- [12] R. Sasaki, Y. Nii, Y. Iguchi, and Y. Onose, *Phys. Rev. B* **95**, 020407 (2017).
- [13] Z. Nazarchuk, V. Skalskyi, and O. Serhiyenko, *Acoustic Emission: Methodology and Application*, Foundation of Engineering Mechanics Series (Springer, Berlin, 2017).
- [14] H. Tsai, S. Karube, K. Kondou, N. Yamaguchi, F. Ishii, and Y. Otani, *Sci. Rep.* **8**, 5564 (2018).
- [15] A. Azevedo, L. H. Vilela-Leão, R. L. Rodríguez-Suárez, A. F. Lacerda Santos, and S. M. Rezende, *Phys. Rev. B* **83**, 144402 (2011).
- [16] K. Ando, S. Takahashi, J. Ieda, Y. Kajiwara, H. Nakayama, T. Yoshino, K. Harii, Y. Fujikawa, M. Matsuo, S. Maekawa, and E. Saitoh, *J. Appl. Phys.* **109**, 103913 (2013).
- [17] See Supplemental Material at <http://link.aps.org/supplemental/10.1103/PhysRevB.97.180301> for full angular variation of spin current, details of fitting formulas for IEE voltage detection, XRD characterization and description of anisotropic distribution of charge potential.
- [18] W. Zhang, M. B. Jungfleisch, W. Jiang, J. E. Pearson, and A. Hoffmann, *J. Appl. Phys.* **117**, 17C727 (2015).
- [19] M. Jamali, J. S. Lee, J. S. Jeong, F. Mahfouz, Y. Lv, Z. Zhao, B. K. Nikolic, K. A. Mkhoyan, N. Samarth, and J.-P. Wang, *Nano Lett.* **15**, 7126 (2015).
- [20] M. Matsuo, J. Ieda, K. Harii, E. Saitoh, and S. Maekawa, *Phys. Rev. B* **87**, 180402 (2013).
- [21] D. Kobayashi, T. Yoshikawa, M. Matsuo, R. Iguchi, S. Maekawa, E. Saitoh, and Y. Nozaki, *Phys. Rev. Lett.* **119**, 077202 (2017).